Magnetoreflectance and magnetization of the Co-based wurtzite-structure diluted magnetic semiconductor $Cd_{1-x}Co_xSe$

F. Hamdani,* J. P. Lascaray, and D. Coquillat
Groupe d'Etude des Semiconducteurs, Université Montpellier II, Place E. Bataillon, 34095-Montpellier CEDEX 5, France

A. K. Bhattacharjee
Laboratoire de Physique des Solides, Université de Paris–Sud, Centre d'Orsay, 91405-Orsay CEDEX, France

M. Nawrocki
Institute of Experimental Physics, University of Warsaw 00-681, Warsaw, Poland

Z. Golacki
Institute of Physics, Polish Academy of Sciences, Aleja Lotnikow 32/46, 02-668 Warsaw, Poland
(Received 8 November 1991)

Magnetoreflectance measurements of excitonic interband transitions in the wurtzite-structure compound $Cd_{1-x}Co_xSe$ with various directions of applied magnetic field combined with magnetization measurements, allowed us to determine the ion-carrier exchange parameters for the conduction and valence bands ($N_0\alpha=258\pm10$ meV, $N_0\beta=-1883\pm30$ meV), without making any assumption concerning the band parameters. The magnitude of these exchange parameters, compared with the values previously obtained for $Cd_{1-x}Fe_xSe$ and $Cd_{1-x}Mn_xSe$, indicates a small variation of the conduction-band exchange parameter, but an important enhancement of the valence-band exchange parameter. This large variation of the hybridization-induced exchange is explained within a generalized Schrieffer-Wolff formula.

I. INTRODUCTION

The family of diluted magnetic semiconductors (DMS) (Ref. 1) has been recently extended through the synthesis of II-VI compounds containing cobalt ions as the magnetic substitute. In accordance with the atomic ground-state degeneracy of Co^{2+} ion, the Co-based DMS (Refs. 2–5) have properties similar to the most extensively studied Mn-based DMS.[1]

The purpose of this paper is to check the validity of the full wurtzite-type Hamiltonian, complete with an exchange term, in the analysis of magnetoreflectivity results of $Cd_{1-x}Co_xSe$, the determination of ion-carrier exchange parameters, and the discussion of the magnitude of these parameters in comparison with Mn- and Fe-based DMS. The atomic ground state of Co^{2+} in a tetrahedral crystal environment is an orbital singlet,[6,7] then the exchange interaction can be described by a spin Hamiltonian,[2] assuming an effective spin $S=\frac{3}{2}$ and taking experimental values of the Landé g factor,[8] which takes into account the orbital contribution leading by the mixing of the ground state with the excited states. In wurtzite DMS compounds, because of the presence of anisotropic spin-orbit and crystal-field interactions, the effect of the magnetic field on the band structure depends on the orientation of the magnetic field relative to the crystal c axis (C). In consequence, the precise determination of ion-carrier exchange parameters $N_0\alpha$ and $N_0\beta$ without any assumption concerning crystal-field (Δ_1) and spin-orbit (Δ_2,Δ_3) parameters, is possible by analyzing the magnetoreflectivity measurements performed for magnetic fields parallel and normal to the crystal axis.

The magnitude of the exchange parameters thus determined compared to iron[9–11] and manganese[12–15] in the same host crystal indicates that $N_0\alpha$, corresponding to the direct-potential exchange interaction (ferromagnetic) remains constant within experimental error. But $N_0\beta$, dominated by kinetic exchange interaction (antiferromagnetic) due to the hybridization of the p valence bands with d orbitals of magnetic ions, increases by increasing the number of electrons in d orbitals of magnetic ions.

II. EXPERIMENTAL DETAILS

$Cd_{1-x}Co_xSe$ crystals with $0\le x\le0.06$ were grown by modified Bridgman technique. The cobalt mole fractions x were checked by microprobe analysis. Some single crystals were oriented with the c axis in the surface plane and some others with the c axis normal to the surface plane. The samples, polished and etched in a 1% bromine in methanol, were placed in a superconducting magnet and immersed in superfluid helium. The maximum field of the magnet was 5.5 T. The magnetoreflectance measurements were performed using a standard experimental setup in both Faraday and Voigt configurations, first with the c axis of the sample parallel to the magnetic field and secondly with the c axis normal to the magnetic-field direction. The magnetization and magnetic susceptibility measurements were carried out by an extraction method in magnetic fields up to 6.5 T oriented parallel and normal to the c axis.

III. MAGNETIZATION MEASUREMENTS

As mentioned above, $Cd_{1-x}Co_xSe$ is a cobalt-based DMS compound with a wurtzite-crystal structure. The free Co^{2+} ion has a $3d^7$ electronic configuration which leads to a $^4F_{9/2}$ ground level. The atomic ground state of Co^{2+} splits under the tetrahedral crystal field and spin-orbit interaction into an orbital singlet $^4A_2$ and two higher-lying triplets $^4T_2$ and $^4T_1$. The ground level is an orbital singlet $^4A_2$ which is split into two Kramers doublets by a trigonal crystal field; this splitting is of the order of 1 K.[6,16] These doublets are separated by about 5.10^3 K from the first excited level $^4T_2$; thus, magnetic properties are controlled by the lowest four states arising from the $^4A_2$ orbital singlet described by an effective spin $S=\frac{3}{2}$ and an anisotropic Landé g factor, which is typically 15% higher than the spin-only value.[5,8] In this case, magnetization data can be described by the modified Brillouin function proposed for manganese DMS compounds:[17]

$$M = MsB_{3/2}(Sg\mu_B H/k_B(T+T_0)) , \quad (1)$$

where $Ms = g\mu_B N_0 \propto S_0$.

The orbital contribution is taken into account by the Landé g factor values ($g_\parallel = 2.295$, $g_\perp = 2.303$),[8] $B_{3/2}$ is a Brillouin function of index $\frac{3}{2}$, S_0 and T_0 are fitting parameters which take into account the antiferromagnetic exchange interaction between magnetic ions associated into a cluster and long-range interactions.

Figure 1 shows the magnetization data of $Cd_{1-x}Co_xSe$ with $x=0.035$ and the magnetic field applied parallel and normal to the c axis; solid curves are the best fits using Eq. (1) and, respectively, the values of $g_\parallel$ and $g_\perp$ factors. We observe a substantial anisotropy of magnetization. The trend of this anisotropy is the same as that of the g factor which results from the small c-axis distortion. But magnetization anisotropy is an order of magnitude larger than the Landé g-factor anisotropy. Our susceptibility results and those previously reported[3] for $Cd_{1-x}Co_xSe$ also exhibit similar anisotropy ($\chi_\perp > \chi_\parallel$). This anisotropy may be explained in terms of spin orbit and Zeeman mixing between ground and excited levels of the Co^{2+} ion in a magnetic field.

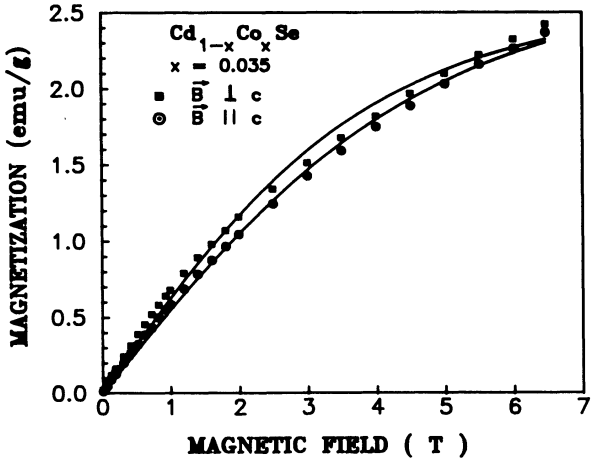

FIG. 1. Magnetization of $Cd_{1-x}Co_xSe$, $x=0.035$, at 1.8 K with magnetic field normal and parallel to the c axis. Solid curves are fit to Eq. (1), with $S_0=1.18$ and $T_0=4.62$ for $\mathbf{B}\parallel c$, $S_0=1.11$, and $T_0=3.52$ for $\mathbf{B}\perp c$.

In agreement with the higher d-d exchange strength revealed in Co-based compounds,[2,3] we note that the values of T_0 are much higher than those of $Cd_{1-x}Mn_xSe$ with the same concentration of magnetic ions.[4] For magnetic field above 3 T, we observe a deviation between experimental results of magnetization and calculated results described by Brillouin function with effective spin $S=\frac{3}{2}$. This deviation, also observed in spin-flip Raman scattering,[5] originates from the contribution of exchange between next-nearest-neighbor ions.[18]

IV. MAGNETOREFLECTIVITY MEASUREMENTS

The valence band of hexagonal $Cd_{1-x}Co_xSe$ compounds is split by means of spin-orbit and crystal-field interactions into three bands which gives rise to A, B, and C excitons. The anisotropy of these interactions induces a mixing of the valence-band states. The valence band, and therefore the exciton transitions, are then affected differently by applying a magnetic field parallel or normal to the crystal-axis (c-axis) direction.

Theoretical analysis of the band structure at the Γ point of the Brillouin zone of wurtzite-structure DMS crystals in the presence of a magnetic field has been previously reported.[12–15] Arciszewska and Nawrocki[12] have pointed out the powerful use of a full wurtzite-type Hamiltonian to study the effect of exchange interactions in the band structure. For a particular case of a magnetic field normal to the crystal c axis ($\mathbf{B}\perp c$), Gubarev[13] has calculated analytic solutions of valence bands. We note that for an arbitrary angle between the magnetic field and the crystal c axis, only numerical solutions can be obtained.[14] The exchange interaction between free carriers in the bands and localized magnetic ions is described by the Kondo Hamiltonian

$$H_{ex} = -\sum_i J^{sp-d}(r-R_i)\mathbf{S}_i\cdot\sigma , \quad (2)$$

where $\mathbf{S}_i$ and σ are the spin operators for the Co^{2+} ion and for the band electron, respectively, J^{sp-d} is the electron-ion $sp-d$ exchange coupling constant, and r and Ri are the coordinates of the band-component electrons and the Co^{2+} ion, respectively. The summation is only over the lattice sites occupied by the Co^{2+} ions. Within the mean-field approximation, we obtain

$$H_{ex} = -\sigma_z\langle S_z\rangle x \sum_i J^{sp-d}(r-R_i) \quad (3)$$

with the summation extending over all cation sites. In consequence, the conduction band with wave functions which have a spherical symmetry at the center of the Brillouin zone is split symmetrically and the spin degeneracy is lifted. The energies of the two conduction-band components are then independent of the magnetic-field direction and given by

$$E^c_{1,2} = E_{g,ex} \pm G_e . \quad (4)$$

$E_{g,\mathrm{ex}}$ is the excitonic energy without magnetic field, $G_e=\frac{1}{2}N_0\alpha x\langle S_z\rangle$ where N_0 is the density of cations, α is the conduction-band exchange integral and $\langle S_z\rangle$ is the magnitude of the thermal average of Co^{2+} spin.

A. Exciton splitting in B||c geometry

In this part, we analyze the results of magnetoreflectivity with a magnetic-field direction parallel to the crystal c axis. Taking the valence-band basis (X_+,X_-,Z) (α,β) where $X_\pm=(X\pm iY)$ and X,Y,Z are functions that transform as the atomic wave functions p_x,p_y, and p_z, respectively; the spin states (α,β) are, respectively, parallel and antiparallel to the z axis which, itself, is assumed to be collinear with the crystal c axis; the eigenvalues of a full wurtzite Hamiltonian, including the Kondo Hamiltonian, are found to be

$$\begin{aligned} E_{A,\pm 3/2}&=\Delta_1+\Delta_2\pm G_h\ , \\ E_{B,\pm 1/2}&=(\Delta_1-\Delta_2)/2+E_\pm\ , \\ E_{C,\pm 1/2}&=(\Delta_1-\Delta_2)/2-E_\mp\ , \end{aligned} \tag{5}$$

corresponding to the energy eigenstates

$$\begin{aligned} &A:\ |\tfrac{3}{2},\pm\tfrac{3}{2}\rangle=|X_\pm(\alpha,\beta)\rangle \\ &B:\ |\tfrac{3}{2},\pm\tfrac{1}{2}\rangle=\pm C_1|X_\pm(\beta,\alpha)\rangle\mp C_2|Z(\alpha,\beta)\rangle \\ &C:\ |\tfrac{1}{2},\pm\tfrac{1}{2}\rangle=C_2|X_\pm(\beta,\alpha)\rangle\pm C_1|Z(\alpha,\beta)\rangle\ . \end{aligned} \tag{6}$$

The energies of the allowed excitonic transitions at the center of the Brillouin zone are

$$\begin{aligned} E_A^{\sigma\pm}&=E_0-\Delta_1-\Delta_2\mp G_e\pm G_h\ , \\ E_B^{\sigma\pm}&=E_0-(\Delta_1-\Delta_2)/2\pm G_e-E_\pm\ , \\ E_B^{\pi}&=E_0-(\Delta_1-\Delta_2)/2\mp G_e-E_\pm\ , \end{aligned} \tag{7}$$

where

$$E_\pm=\left[\left[\frac{(\Delta_1-\Delta_2)\pm 2G_h}{2}\right]^2+2\Delta_3^2\right]^{1/2}\ .$$

Δ_1 is the crystal-field splitting constant and Δ_2 and Δ_3 are the constants of spin-orbit interactions. $(E_0-\Delta_1-\Delta_2)$ is the energy of the ground state of the A excitonic transition, without magnetic field. $G_h=\frac{1}{2}N_0\beta x\langle S_z\rangle$, where β is the valence-band exchange integral. Equations related to C-exciton transitions that are not experimentally observed are omitted. In the presence of a magnetic field, the exchange interaction splits every previous band into two subbands. In the case of the $m_j=\pm\frac{3}{2}$ levels (A exciton), the splitting is proportional to the thermal average of Co^{2+} spins per cation, $x\langle S_z\rangle$. However, the functional dependence in the $m_j=\pm\frac{1}{2}$ cases is much more complicated because of the mixing of spin ($\frac{1}{2}$) basis by the combined action of the crystal field, spin-orbit interactions characteristic of wurtzite structure, and the exchange-interaction characteristic of DMS and gives rise to asymmetric splitting of the B and C excitons.

Magnetoreflectivity measurements have been carried out in both Faraday and Voigt configurations for cobalt concentrations lower than $x=0.06$. The slope of the variation of fundamental excitonic transitions with concentration is higher for $Cd_{1-x}Co_xSe$ than for the $Cd_{1-x}Mn_xSe$ compound; this is probably due to the higher value of the energy gap of the hypothetical wurtzite CoSe compared to MnSe.

In Figs. 2(a) and 2(b), magnetoreflectivity spectra of $Cd_{1-x}Co_xSe$ with $x=0.035$ are shown at a temperature of 1.8 K in different magnetic fields in the Voigt

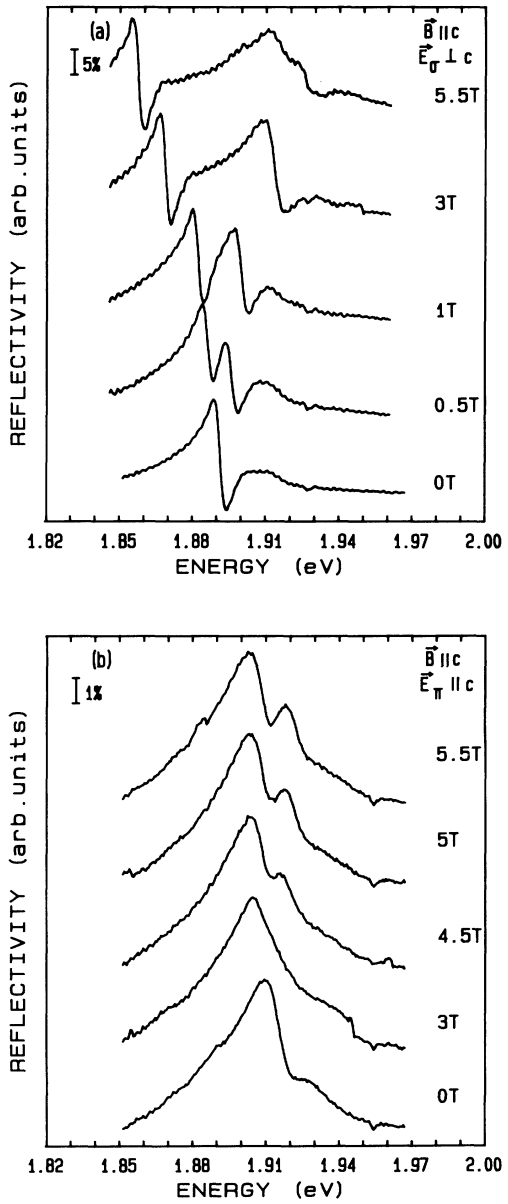

FIG. 2. (a) Magnetoreflectance spectra for $Cd_{1-x}Co_xSe$, $x=0.035$, at 1.8 K in Voigt configuration with $\mathbf{B}\|c$ and $\mathbf{E}_\sigma\perp c$. (b) Magnetoreflectance spectra for $Cd_{1-x}Co_xSe$, $x=0.035$, at 1.8 K in Voigt configuration with $\mathbf{B}\|c$ and $\mathbf{E}_\pi\|c$.

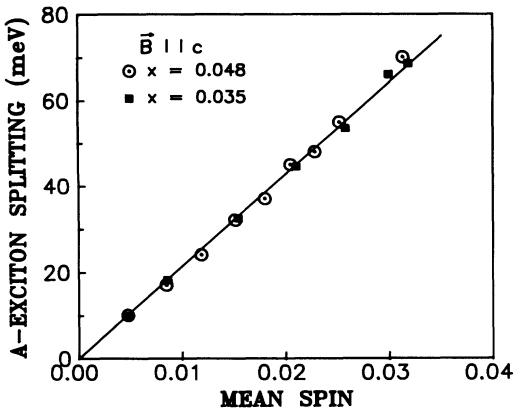

FIG. 3. Energy splitting of A-excitonic transitions vs the mean value of Co^{2+} spin with $\mathbf{B}\|c$ for two different concentrations of cobalt ions ($x=0.035$ and $x=0.048$). The straight line of slope 2148 meV is adjusted to best fit the data.

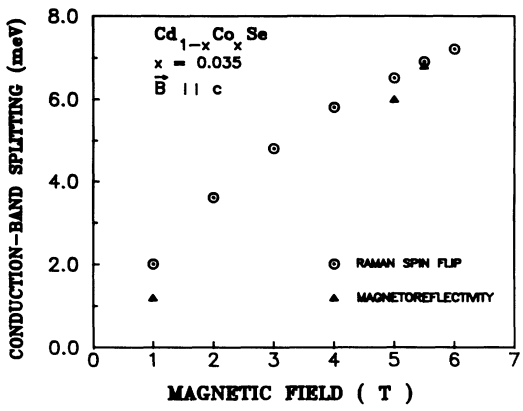

FIG. 5. Conduction-band splitting deduced from magnetoreflectance data with $\mathbf{B}\|c$ (triangles) compared to results obtained by the spin-flip Raman-scattering technique by Bartholomew *et al.* in Ref. 5 for the same concentration of cobalt $x=0.035$.

configuration ($\mathbf{k}\perp\mathbf{B}$, $\mathbf{B}\|c$). Figure 2(a) shows magnetoreflectivity spectra with a light electric vector normal to the c axis $\mathbf{E}\perp c$ (E_σ). All four transitions ($\Delta m_j=\pm1$) are allowed: two A-exciton components and two B-exciton ones. The A-exciton splitting is very large and well observed. The B-exciton splitting is very small and we can observe only a single broad transition; it can be attributed to the high-energy component of the B exciton, whose oscillator strength increases with magnetic field. By increasing the magnetic field, the crossing of B-exciton levels with the high-energy A-exciton level is observed.

Figure 2(b) shows magnetoreflectivity spectra of the same sample $x=0.035$ in the Voigt configuration with $\mathbf{E}\|c$ (E_π). In this case the A-exciton transitions are forbidden and we observe only the splitting of the B exciton. The spectra indicate the perfect orientation of the c axis in the direction of the magnetic field because no parasite transitions from the A exciton is observed.

In Fig. 3 the splitting of the A exciton versus $x\langle S_z\rangle$ allows the determination of $N_0(\alpha-\beta)$. The value deduced by the best fit of the data taken for different concentrations is $N_0(\alpha-\beta)=2141\pm20$ meV. By the analysis of results obtained in both Faraday and Voigt configurations in ($\mathbf{B}\|c$) geometry it is possible to determine the conduction-band exchange parameter by means of B-exciton transitions from a given valence subband to the two different conduction subbands. We can then estimate the conduction-band splitting:

$$\Delta E_c=N_0\alpha x\langle S_z\rangle=E_{B2}^{\pi}-E_B^{\sigma-}=E_B^{\sigma+}-E_{B1}^{\pi}\ , \qquad (8)$$

where E_{B1}^{π} (E_{B2}^{π}) is the lower (higher) energy transition arising from the B exciton in the Voigt configuration (see Fig. 4). The exchange parameters deduced by this procedure are less accurate because of the broad B-excitonic transitions. In Fig. 5, we have compared the conduction-band splitting deduced by this procedure [Eq. (8)] and those deduced from spin-flip Raman scattering given by Bartholomew *et al.*[5] for the same cobalt concentration $x=0.035$.

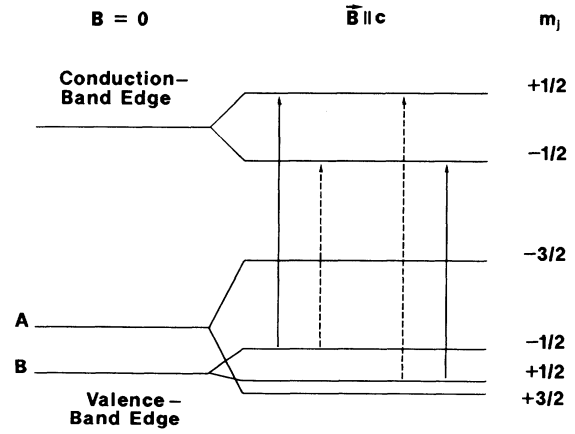

FIG. 4. Schematic diagram of band splitting in the case of $\mathbf{B}\|c$. Allowed optical transitions arising from the B exciton are indicated by solid lines in the Faraday configuration and by dashed lines in the Voigt configuration.

B. Excitonic splitting in $\mathbf{B}\perp c$ geometry

As noted in the previous section, the exchange splitting of the conduction band is only affected by the magnitude of the magnetic field, whereas the valence subbands are affected also by the direction of the magnetic field with respect to the crystal c axis. This anisotropic variation of the valence band is induced by the exchange interaction between magnetic ions and band carriers. The mixing of valence subbands dependent on the magnetic field is then caused by the exchange interaction and changes the symmetry of valence-band states, selection rules, and optical excitonic transition probabilities. We follow the analysis and notation given by Gubarev in Ref. 13. We consider the magnetic-field direction along the x axis and the crystal axis along the z axis and we use for the valence bands a wave-function basis with the spin quantization axis along the magnetic field ($x\alpha'$, $iy\beta'$, $z\beta'$, $x\beta'$, $iy\alpha'$, $-z\alpha'$), where $\alpha'=(\alpha+\beta)$ and $\beta'=(\beta-\alpha)$ are the transforma-

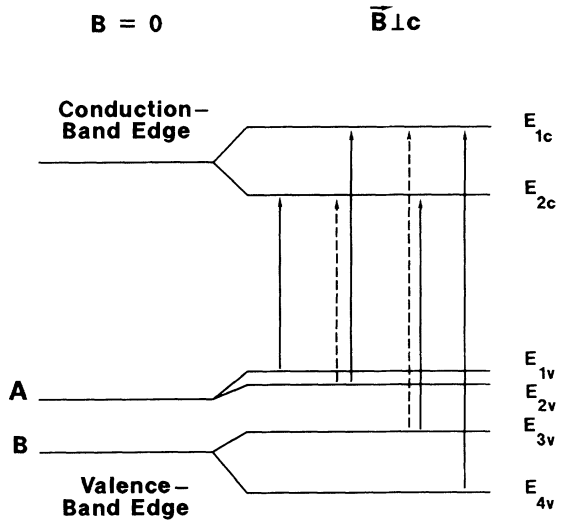

FIG. 6. Schematic diagram of band splitting in the case of $\mathbf{B}\perp c$. Allowed optical transition with light electric vector direction along $\mathbf{E}_x$ are indicated by dashed lines and those with $\mathbf{E}_y$ and $\mathbf{E}_z$ are indicated by solid lines.

tions of the spin variables. On this basis the total Hamiltonian composed of the full-band Hamiltonian (H_0) and the exchange Hamiltonian (H_{ex}) can be written as

$$H=H_0+H_{ex}=\begin{bmatrix} L_1 & 0 \\ 0 & L_1 \end{bmatrix}, \tag{9}$$

$$L_1=\begin{bmatrix} -\Delta_2-G_h & -\Delta_2 & \Delta_3 \\ -\Delta_2 & -\Delta_2+G_h & \Delta_3 \\ \Delta_3 & \Delta_3 & -\Delta_1-\Delta_2+G_h \end{bmatrix}.$$

Six solutions ($E_i, i=1,2,\ldots,6$) of the secular equation for the total Hamiltonian are then deduced and eigenfunctions corresponding to these energies are given as the following linear combinations of the basis functions:

For $i=1,3,5$

$$\Psi_i=C_x^i(x\alpha')+C_y^i(iy\beta')+C_z^i(z\beta')$$

and for $i=2,4,6$

$$\Psi_i=C_x^i(x\beta')+C_y^i(iy\alpha')-C_z^i(z\alpha'),$$

with

$$\sum_{u=x,y,z}(C_u^i)^2=1 .$$

The optical-transition probabilities (f_u^{ij}) between the valence band Ψ_{vi} and the conduction band Ψ_{cj} in the polarization $u=x,y,z$ are determined by the square of the coefficients (C_u^i) which depend on exchange energies (G_h) and band parameters ($\Delta_1,\Delta_2,\Delta_3$).

$$f_u^{ij}=(C_u^i)^2\delta_{\sigma i\sigma j} . \tag{10}$$

δ is the Kronecker symbol; σi (σj) the spin state associated with the valence band (conduction band).

The scheme of energetic levels and allowed transitions for the $\mathbf{B}\perp c$ configuration is presented in Fig. 6. Figure 7 shows the relative probabilities of allowed transitions for different linear polarizations as a function of the magnetic field calculated by Eq. (10) and using magnetization data presented in Sec. III.

Figures 8–10 show magnetoreflectance spectra for the same sample of $Cd_{1-x}Co_xSe$ with $x=0.035$ at 1.8 K for different values of the magnetic field applied normal to the crystal c axis and for different linear polarizations. In Fig. 8 magnetoreflectance spectra of $Cd_{1-x}Co_xSe$ are shown in the case of $\mathbf{B}\perp c$ and $\mathbf{E}\|c$ ($\mathbf{E}_z$). In the absence of a magnetic field, only a single transition attributed to the B exciton is observed, A-exciton transition is forbidden in this polarization. By applying a magnetic field, the A-exciton transitions appear and become allowed as a result of the wave-function mixing between the three valence bands (A, B, and C) by means of exchange interaction. This is consistent with an increase in oscillator strength with increasing magnetic field in this polarization shown in Fig. 7. At magnetic fields above 2 T, we clearly observe two transitions arising from the A valence bands. This splitting is mainly due to the conduction-band splitting and also to a small A-valence-band splitting induced

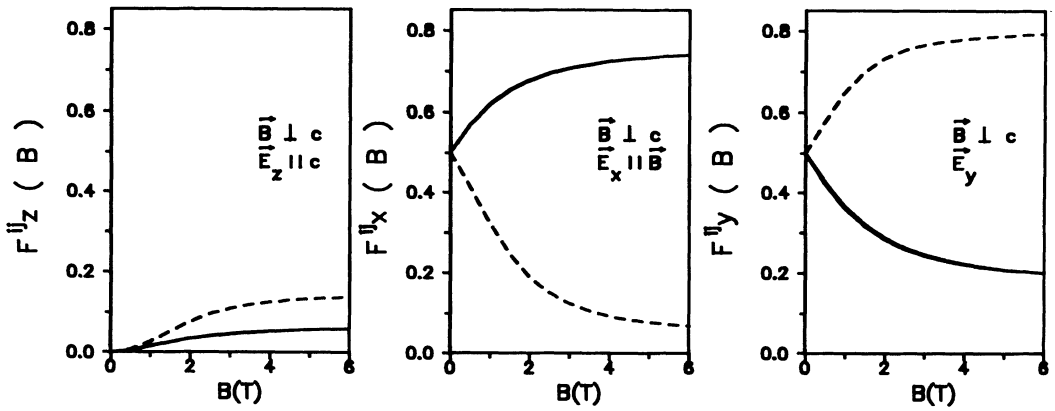

FIG. 7. Relative probabilities of optical transitions with different directions of light electric vectors vs magnetic field in the case of $\mathbf{B}\perp c$. Solid (dashed) lines correspond to transitions between A-valence bands and conduction band $|\frac{1}{2},\frac{1}{2}\rangle(|\frac{1}{2},-\frac{1}{2}\rangle)$.

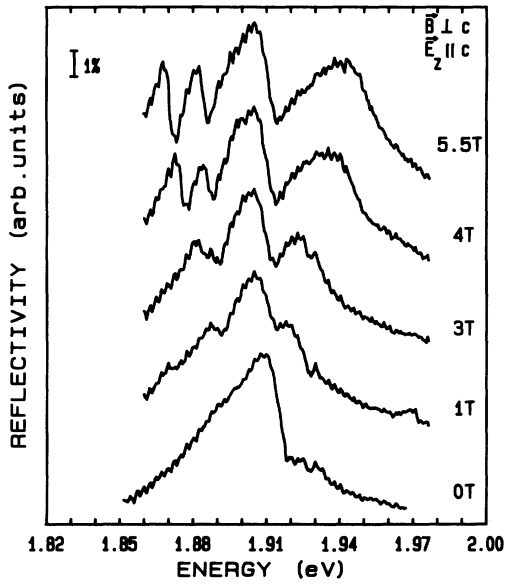

FIG. 8. Magnetoreflectance spectra of $Cd_{1-x}Co_xSe$, $x=0.035$, at 1.8 K with $\mathbf{B}\perp c$ and the light electric vector direction (E) parallel to the crystal c axis ($\mathbf{E}_z\|c$).

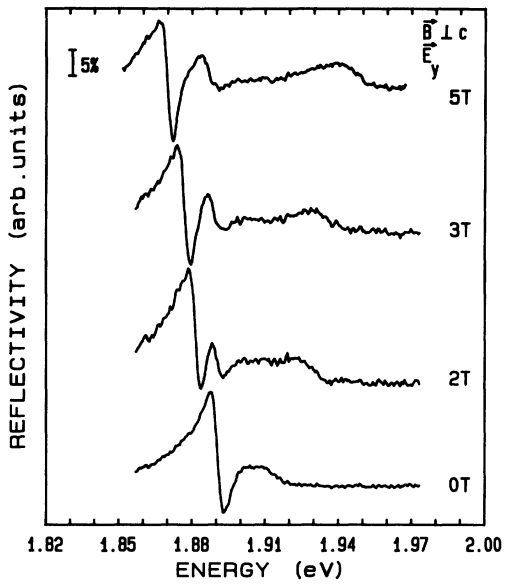

FIG. 10. Magnetoreflectance spectra of $Cd_{1-x}Co_xSe$, $x=0.035$, at 1.8 K with $\mathbf{B}\perp c$, $\mathbf{E}_y\perp\mathbf{B}$, and $\mathbf{E}_y\perp c$.

by the mixing of valence bands. The center of gravity of A-exciton transitions is shifted towards lower energies relative to the energy position without a magnetic field.

In Fig. 8, we also observe a large splitting of B-exciton transitions, indicating a large splitting of B valence bands in this configuration ($\mathbf{B}\perp c$), the center of gravity of B-excitonic transition is shifted towards higher energies so that no crossing is observed between the A- and B-excitonic transitions.

Figure 9 shows magnetoreflectance spectra with $\mathbf{B}\perp c$ and $\mathbf{E}\|\mathbf{B}$ ($\mathbf{E}_x$) for different magnetic fields; we observe only two excitonic transitions. The well-defined transition at the low-energy side is attributed to the A-exciton band; the second A-exciton transition is not observed, in agreement with the calculated transition probabilities that indicate that in this polarization the oscillator strength of the high-energy A-excitonic transition is dropped by increasing the applied magnetic field (see Fig. 7). The same remarks are used to analyze the B-exciton transitions.

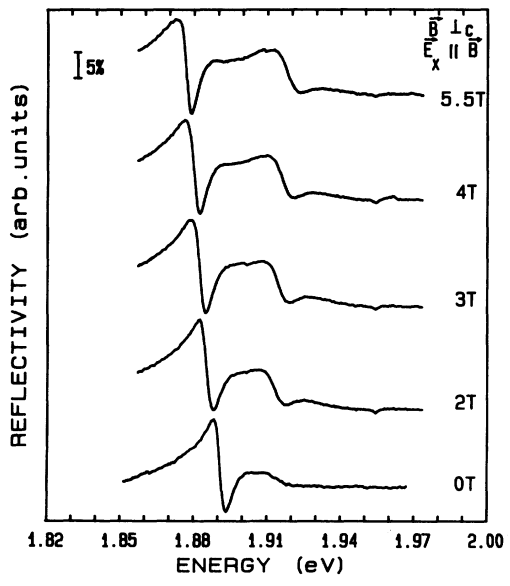

FIG. 9. Magnetoreflectance spectra of $Cd_{1-x}Co_xSe$, $x=0.035$, at 1.8 K with $\mathbf{B}\perp c$ and $\mathbf{E}_x\|\mathbf{B}$.

Figure 10 shows magnetoreflectance spectra with $\mathbf{B}\perp c$, $\mathbf{E}\perp c$ and $\mathbf{E}\perp\mathbf{B}$ ($\mathbf{E}_y$). At the low-energy side two excitonic transitions attributed to the A exciton are well observed, consistent with calculated transition probabilities shown in Fig. 7. The energy positions of these peaks are the same as those for A-exciton transitions observed in Fig. 8 with $\mathbf{E}_z\|c$. Only one transition attributed to the B exciton is observed in the present configuration.

The excitonic interband transitions observed in these experiments are shown in Fig. 6 as vertical lines connecting the appropriate A or B valence band to conduction-band levels, all of which are shown split by the action of an applied magnetic field normal to the c axis. The identification of these transitions is according to calculated energy positions and transition probabilities. We note that there are allowed transitions from a given valence subband to the two different conduction-band components. The observation of these transitions allows direct determination of conduction-band splitting and thus the exchange parameter $N_0\alpha$:

$$\Delta\mathbf{E}_c = E^{y,z}_{A21} - E^{x}_{A22} = E^{x}_{B31} - E^{y,z}_{B32} , \tag{11}$$

where E^u_{ij} is the excitonic transitions between the valence band Ψ_i and the conduction band Ψ_j with the light electric vector oriented along the (u) direction (see Fig. 6).

Figure 11 shows the conduction-band splitting ΔE_c obtained from Eq. (11), versus $x\langle S_z\rangle$ deduced from magne-

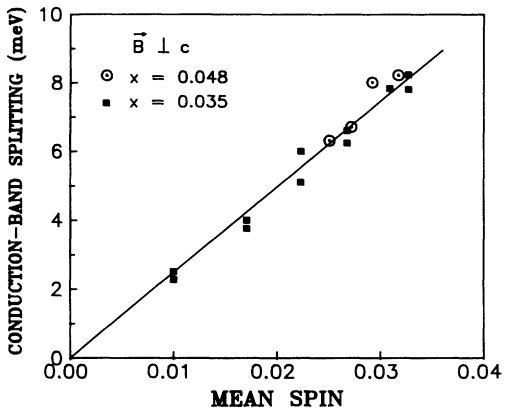

FIG. 11. Conduction-band splitting vs the mean value of Co^{2+} spin with $\mathbf{B}\perp c$. The straight line of slope 258 meV is adjusted to best fit the data.

tization data with $\mathbf{B}\perp c$ and taking $g_\perp = 2.303$. A best-fit straight line of slope 258 ± 10 meV shows the linear relationship between the two quantities. The conduction-band splitting at 5.5 T is weaker than the value deduced in the preceding section with $\mathbf{B}\|c$; this is explained by the anisotropy of magnetization observed above. The exchange integral for the valence band is then determined using the value of $N_0(\alpha-\beta)$ obtained in Sec. IV A. In this manner the exchange parameters are determined without making any assumption concerning the band parameters.

$$N_0\alpha = 258\pm10 \text{ meV}, \quad N_0\beta = 1883\pm30 \text{ meV} .$$

The values of band parameters are deduced, on the other hand, by fitting the variation of excitonic transitions in $\mathbf{B}\|c$ geometry using Eq. (7) and the exchange parameters obtained above (Fig. 12). We obtain

$$\Delta_1 = 80\pm10 \text{ meV}, \quad \Delta_2 = 133\pm23 \text{ meV},$$

$$\Delta_3 = 150\pm2 \text{ meV}$$

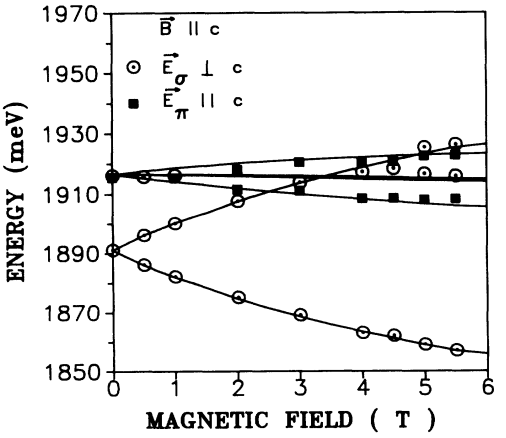

FIG. 12. Energy of A and B excitons vs magnetic field in $\mathbf{B}\|c$ geometry. The lines are the fit to Eq. (7); the only fitting parameters are the three-band parameters Δ_1, Δ_2, and Δ_3.

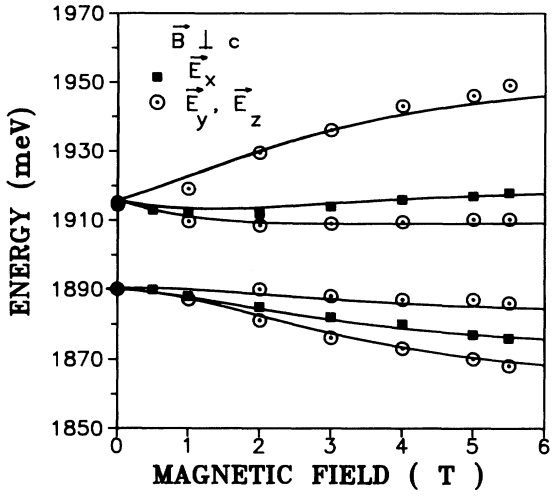

FIG. 13. Excitonic transition energies plotted vs the magnetic field in the case of $\mathbf{B}\perp c$ and compared to calculated transitions energies indicated by solid lines.

These values are close to the values reported for $Cd_{1-x}Mn_xSe$.[12–15] We have used these values of band parameters and the data of magnetization experiments to calculate the variation of exciton energy versus magnetic field normal to the crystal-field axis. Figure 13 shows good agreement between experimental results and theoretical curves. The theoretical calculations are done without any adjustable parameters.

V. VARIATION OF CARRIER-ION EXCHANGE WITH THE TRANSITION-METAL ION

Together with our results, a set of available $N_0\alpha$ and $N_0\beta$ values are presented in Table I, showing the variation of exchange parameters with the transition-metal ion in the CdSe host. Clearly, the overall variation of $N_0\alpha$ is rather small. But $|N_0\beta|$ increases systematically as one passes from Mn^{2+} to Fe^{2+} to Co^{2+}.

Here we present an explanation of this variation by extending the analysis of Ref. 19 to the case of n electrons in the d shell with $n = 5, 6$, and 7, for Mn^{2+}, Fe^{2+}, and Co^{2+}, respectively. The relatively weak ferromagnetic (positive) $N_0\alpha$ corresponds to the ordinary "potential" exchange. For an s-like conduction band, it is expected to vary little with the number of electrons in the d shell.[20]

TABLE I. Carrier-ion exchange parameters of $Cd_{1-x}M_xSe$ with M = Mn, Fe, and Co; $(E_v - \varepsilon_d)$ and U_{eff} are parameters estimated using photoemission data (Refs. 25 and 28).

	$Cd_{1-x}Mn_xSe$	$Cd_{1-x}Fe_xSe$	$Cd_{1-x}Co_xSe$
$N_0\alpha$ (meV)	261[a]	250[b]	258
$N_0\beta$ (meV)	−1238[a]	−1450[c]	−1883
$E_v - \varepsilon_d$ (eV)	3.4[d]	3.7[e]	3.5[f]
U_{eff} (eV)	7.6[d]	6.8	5.9

[a]Reference 12.
[b]Reference 30.
[c]Reference 9.
[d]Reference 22.
[e]Reference 25.
[f]Reference 28.

Indeed, experimental $N_0\alpha$ values in Table I show only a small variation. On the other hand, the strong antiferromagnetic (negative) $N_0\beta$ is dominated by "kinetic" exchange arising from the hybridization of d orbitals with the anion p-like valence-band states. For the S-state ion Mn^{2+}, neglecting direct exchange, it is given by the generalized Schrieffer-Wolff formula:[21]

$$N_0\beta=-\frac{1}{2S}32V_{pd}^2[(E_v-\varepsilon_d)^{-1}+(\varepsilon_d+U_{\text{eff}}-E_v)^{-1}] \tag{12}$$

in the usual notations (see, for example, Ref. 22). In general, for a non-S-state ion, hybridization yields not only the spin-spin exchange term retained above but also orbital exchange terms. However, the latter are quenched in the case of Fe^{2+} and Co^{2+} ions in tetrahedral symmetry.[23] In the strong crystal-field coupling scheme, the respective ground states ^5E and $^4A_2$ belong to the configurations $e^3t_2^3$ and $e^4t_2^3$. Thus, in all three cases, every t_2 orbital is singly occupied. As only t_2 orbitals hybridize with the valence band at the center of Brillouin zone, Eq. (12) is valid for Fe^{2+} and Co^{2+} as well.[24]

A comparative analysis of photoemission experiments[25] in $Cd_{1-x}Fe_xSe$ and $Cd_{1-x}Mn_xSe$ allows an estimate of the energy denominators in Eq. (12). First of all, $(E_v-\varepsilon_d)\simeq 3.7$ eV for Fe^{2+}, compared with 3.4 eV for Mn^{2+}. Moreover, the minority-spin occupied level in Fe^{2+} lies about 3.2 eV above the majority-spin level. Now, within the (U,U',J) model of Kanamori discussed in Ref. 26, this energy corresponds to $4J$. On the other hand, U_{eff} decreases by J in passing from Mn^{2+} to Fe^{2+}. Thus, assuming $U_{\text{eff}}=7.6$ eV (Ref. 22) for Mn^{2+}, the value for Fe^{2+} should be $\simeq 6.8$ eV. With the above energy values the sum in the square bracket in Eq. (12) increases by 11% from Mn^{2+} to Fe^{2+}. Using the appropriate S values in Eq. (12) the observed increase of $|N_0\beta|$ from $Cd_{1-x}Mn_xSe$ to $Cd_{1-x}Fe_xSe$ then suggests a decrease of V_{pd}^2 by $\sim 16\%$. This is not surprising. According to Harrison's rule,[27] V_{pd}^2 is proportional to (r_d^3/d^7). With the tabulated values[27] the decrease of d-shell radius r_d from 0.86 to 0.80 Å predicts a decrease of V_{pd}^2 by 20% if the Fe-Se bond length d is assumed to be the same as the Mn-Se one.

A similar analysis based on the photoemission data[28] of $Cd_{1-x}Co_xSe$ leads to an even better agreement between Eq. (12) and the relative value of $N_0\beta$ in the case of Co^{2+}. However, the quantitative agreement should not be taken too seriously. There are considerable uncertainties in the interpretation of photoemission spectra and, in particular, in the estimated values of U_{eff} shown in Table I. Moreover, no extended x-ray-absorption fine-structure (EXAFS) information on bond length is available in Fe- or Co-based DMS.

To conclude this discussion we emphasize the following points. Contrary to previous interpretation,[29] the hybridization parameter V_{pd} decreases from Mn^{2+} to Fe^{2+} to Co^{2+}. The resulting decrease of $|N_0\beta|$ is more or less compensated by the increase coming from reduced U_{eff} values. The scaling factor $1/2S$ in Eq. (12), which is then crucial for explaining the large increase of $|N_0\beta|$, seems to have been ignored so far.

VI. CONCLUSIONS

We have performed magnetization and magnetoreflectivity measurements in wurtzite semimagnetic semiconductor $Cd_{1-x}Co_xSe$, with applied magnetic fields parallel and perpendicular to the c axis. The eigenvalues of a wurtzite-type Hamiltonian, complete with an exchange term, describe very closely the variation of exciton energies with magnetic fields, in both $\mathbf{B}\|c$ and $\mathbf{B}\perp c$ geometry. Through a judicious choice of geometry in the magnetoreflectivity experiments with $\mathbf{B}\perp c$, we have measured directly the conduction-band splitting. Combining magnetization and magnetoreflectivity data, we thus obtain accurate values for the ion-carrier exchange constants: $N_0\alpha=258\pm 10$ meV, $N_0\beta=-1883\pm 30$ meV. Comparison with $Cd_{1-x}Mn_xSe$ and $Cd_{1-x}Fe_xSe$ reveals a large increase of $|N_0\beta|$ from Mn to Fe to Co in the CdSe host. This has been explained within the Schrieffer-Wolff framework.

ACKNOWLEDGMENTS

We are grateful to J. Deportes for performing magnetization measurements at Louis Neel laboratory of Grenoble. Groupe d'Etudes des Semiconducteurs is "Unité Associée No. 357 du Centre National de la Recherche Scientifique" and Laboratoire de Physique des Solides is "Unité Associée No. 2 du Centre National de la Recherche Scientifique."

*On leave from Unité de Developpement de la Technologie du Silicium, Ministère Délégué à la Recherche et à la Technologie, Algiers, Algeria.

[1] *Diluted Magnetic Semiconductors, Semiconductors and Semimetals,* edited by J. K. Furdyna and J. Kossut (Academic, Boston, 1988), Vol. 25.

[2] T. M. Giebultowicz, P. Klosowski, J. J. Rhyne, T. J. Udovic, J. K. Furdyna, and W. Giriat, Phys. Rev. B **41**, 504 (1990); T. M. Giebultowicz, J. J. Rhyne, J. K. Furdyna and P. Klosowski, J. Appl. Phys. **67**, 5096 (1990).

[3] A. Lewicki, A. I. Schindler, J. K. Furdyna, and W. Giriat, Phys. Rev. B **40**, 2379 (1989); A. Lewicki, A. I. Schindler, I. Miotkowski, and J. K. Furdyna, *ibid.* **41**, 4653 (1990).

[4] M. Nawrocki, F. Hamdani, J. P. Lascaray, Z. Golacki, and J. Deportes, Solid State Commun. **77**, 111 (1991).

[5] D. U. Bartholomew, E. K. Suh, A. K. Ramdas, S. Rodrigues, U. Debska, and J. K. Furdyna, Phys. Rev. B **39**, 5865 (1989); A. K. Ramdas, in *High Magnetic Fields in Semiconductor Physics II,* edited by Gottfried Landwehr, Springer Series in Solid State Sciences Vol. 87 (Springer-Verlag, New York, 1989), p. 464.

[6] H. A. Weakliem, J. Chem. Phys. **36**, 2117 (1962).

[7] M. Villeret, S. Rodriguez, and E. Kartheuser, J. Appl. Phys. **67**, 4221 (1990).

[8] T. Hoshina, J. Phys. Soc. Jpn. **21**, 1608 (1966).

[9] O. W. Shih, R. L. Aggarwal, Y. Shapira, S. H. Bloom, V. Bin-

dilatti, R. Kershaw, K. Dwight, and A. Wold, Solid State Commun. **74**, 455 (1990).
[10]A. Twardowski, K. Pakula, I. Perez, P. Wise, and J. E. Crow, Phys. Rev. B **42**, 7567 (1990).
[11]D. Scalbert, M. Guillot, A. Mauger, J. A. Gaj, and J. Cernogora, Solid State Commun. **76**, 977 (1990).
[12]M. Arciszewska and M. Nawrocki, J. Phys. Chem. Solids **47**, 309 (1986).
[13]S. I. Gubarev, Phys. Status Solidi B **134**, 211 (1986); J. Cryst. Growth **101**, 882 (1990).
[14]R. L. Aggarwal, S. N. Japerson, J. Stankiewicz, Y. Shapira, S. Foner, B. Khazia, and A. Wold, Phys. Rev. B **28**, 6907 (1983).
[15]A. V. Komarov, S. M. Ryabchenko, Yu. G. Semenov, B. D. Shanina, and N. I. Vitrikovski, Zh. Eksp. Teor. Fiz. **79**, 1554 (1980) [Sov. Phys. JETP **52**, 783 (1980)].
[16]A. Lewicki, A. I. Schindler, I. Miotkowski, B. C. Crooker, and J. K. Furdyna, Phys. Rev. B **43**, 5713 (1991).
[17]J. A. Gaj, R. Planel, and G. Fishman, Solid State Commun. **29**, 435 (1979).
[18]Y. Shapira, J. Q. Wu, B. K. Lau, S. Foner, E. J. McNiff, D. Heiman, C. L. H. Thieme, C. M. Niu, R. Kershaw, K. Dwight, A. Wold, and V. Bindilatti, Solid State Commun. **75**, 201 (1990).
[19]A. K. Bhattacharjee, G. Fishman, and B. Coqblin, Physica **117/118**, 449 (1983).
[20]S. H. Liu, Phys. Rev. **121**, 451 (1961).
[21]J. R. Schrieffer, J. Appl. Phys. **38**, 1143 (1967).
[22]B. E. Larson, K. C. Hass, H. Ehrenreich, and A. E. Carlsson, Phys. Rev. B **37**, 4137 (1988).
[23]J. Blinowski and P. Kacman, in *Proceedings of the 20th International Conference on the Physics of Semiconductors,* edited by E. M. Anastassakis and J. D. Joannopoulos (World Scientific, Singapore, 1990), p. 1827.
[24]A. K. Bhattacharjee (unpublished).
[25]M. Taniguchi, Y. Ueda, I. Morisada, Y. Murashita, and Y. Oka, Phys. Rev. B **41**, 3069 (1990).
[26]K. C. Hass, in *Semimagnetic Semiconductors and Diluted Magnetic Semiconductors,* edited by M. Averous and M. Balkanski (Plenum, New York, 1991), Vol. 55, p. 59.
[27]W. A. Harrison, *Electronic Structure and the Properties of Solids* (Freeman, San Francisco, 1980).
[28]K. Kopalko, B. J. Kowalski, B. A. Orlowski, A. Mycielski, and V. Chab, Acta Phys. Pol. A **77**, 403 (1990).
[29]A. Twardowski, K. Pakula, I. Perez, P. Wise, and J. E. Crow, Phys. Rev. B **42**, 7567 (1990).
[30]D. Scalbert, J. A. Gaj, A. Mauger, J. Cernogora, and C. Benoit à la Guillaume, Phys. Rev. Lett. **62**, 2865 (1989); D. A. Heiman, A. Petrou, S. H. Bloom, Y. Shapira, E. D. Isaacs, and W. Giriat, *ibid.* **60**, 1876 (1988).